Heliyon 10 (2024) e36784

Contents lists available at ScienceDirect

Heliyon

journal homepage: www.cell.com/heliyon

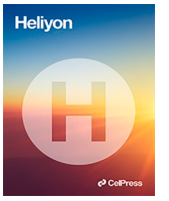

Research article

Controllable synthesize of ZnS/PbS nanostructure and their structural and morphological properties

Bassem Assfour [a,*], Bassam Abadllah [b], Nada Daoud [a], Mahmoud Kakhia [b], Walaa Zetoun [b]

[a] Atomic Energy Commission, Department of Chemistry, P. O. Box 6091, Damascus, Syria
[b] Atomic Energy Commission, Department of Physics, P. O. Box 6091, Damascus, Syria

ARTICLE INFO

Keywords:
ZnS nanowire
Thermal evaporation
Ion doping
HRSEM
HRTEM

ABSTRACT

ZnS is an appealing material with wide potential applications in optoelectronics, sensors, and photocatalysis due to its fascinating properties, low cost, and eco-friendly. In this paper, we report the synthesis of ZnS nanowires and nanorods via a simple thermal-evaporation method using different concentrations of PbS as a dopant. The prepared nanostrutures were investigated in detalis using a scanning electron microscopy (SEM), X-ray diffraction (XRD), and high resolution transmission electron microscopy (HRTEM). The results show that the fabricated ZnS nanowire/nanorod has a wurtzite (hcp) structure. In addition, based on the experimental results, the growth mechanism of the prepared nanostructures is reported. X-ray photoelectron spectroscopy (XPS) and energy-dispersive X-ray (EDX) mapping analyses confirmed that the ZnS nanorods were stoichiometric without impurities or defects, whereas PbS quantum dots were formed inside the high-quality nanowires. The formation mechanism of ZnS nanowires is discussed based on the vapor–liquid–solid (VLS) growth model. Results demonstrated that thermal evaporation is a simple and effective techniques for producing high-quality heterostructured ZnS nanowires with potential applications in different fields.

1. Introduction

ZnS is a intensively studied semiconductor with wide potential applications [1]. Recent developments in ZnS research include optoelectronics, nonlinear optical absorption [2], photocatalysis [3] and dye-sensitized solar cells [4]. It has a wide direct bandgap (3.54, 3.91 eV) depending on the structure, excellent chemical and thermal stability, and a large exciton binding energy (39 meV at room temperature). The band gap of ZnS can be controlled via doping or nanostructuring [5,6].

ZnS can be doped with various elements in order to modify its properties. For example, doping with transition metals such as Mn, Pb, Ni, Cu, or V can change their luminescence characteristics [7,8]. Doping with non-metals such as N, P, or As can alter their electrical conductivities [9,10]. Doping with other elements such as Ag or In can enhance the scintillation efficiency of ZnS. Similar results have been reported by other groups for the doping of ZnS using different elements.

PbS exhibits dual functionality as both a catalyst and a dopant for ZnS. In case of catalyst, PbS influences the growth mechanism of ZnS films during deposition, acting as a buffer layer that facilitates the formation of ZnS nanostructures [11]. The growth of ZnS nanorods or nanowires via a vapor–liquid–solid (VLS) process is enhanced in the presence of the PbS catalyst via the formation of

* Corresponding author.
E-mail address: cscientific15@aec.org.sy (B. Assfour).

https://doi.org/10.1016/j.heliyon.2024.e36784
Received 8 July 2024; Received in revised form 22 August 2024; Accepted 22 August 2024
Available online 29 August 2024

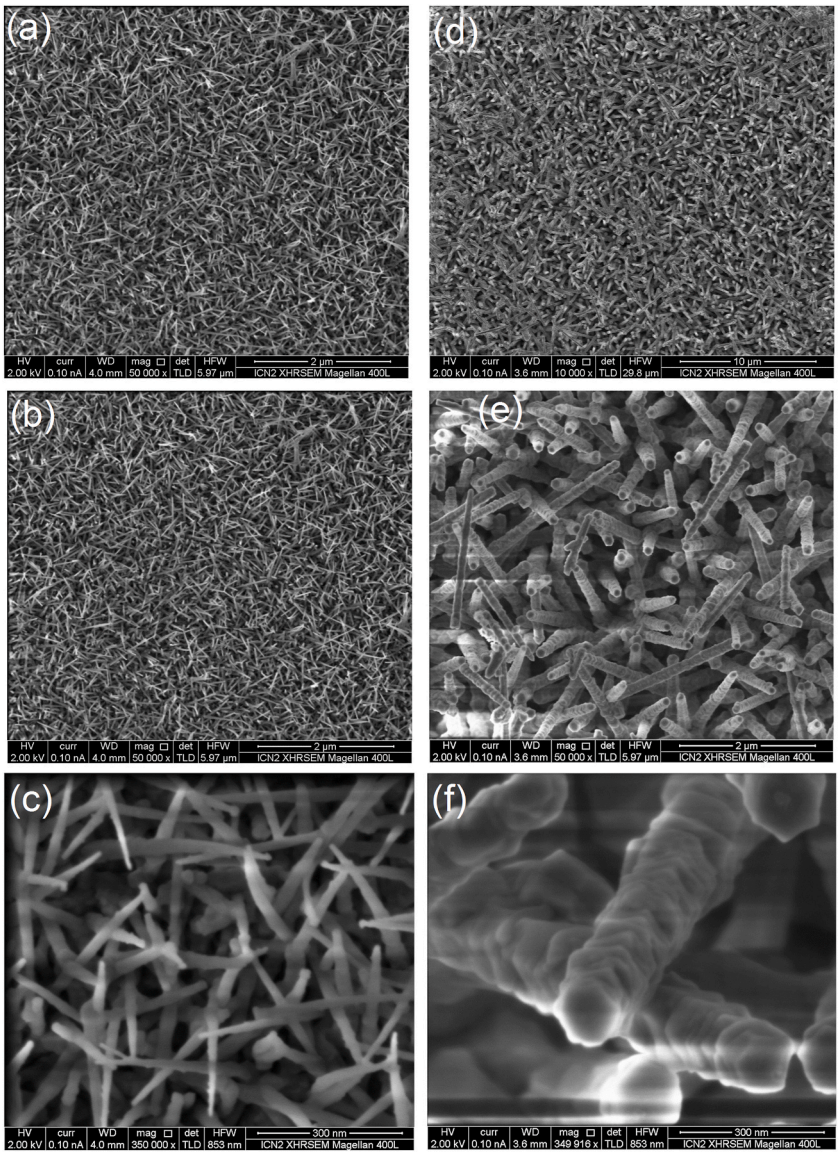

Fig. 1. SEM images of the obtained ZnS nanomaterial with different magnifications. Left-hand side (a–c): sample deposited on Silicon substrate (ZnS/Si) - PbS wt. 12 % (Nanowires); right-hand side (e–f): sample deposited on glass substrate (ZnS/glass) - PbS wt. 6 % (Nanorods); top: 10k magnification– 10 μm; middle: 50k magnification – 2 μm; bottom: 350k magnification – 300 nm.

supersaturated alloy droplets [12,13].

PbS can also be used as a ZnS dopant. This method enhances the photoluminescence and stability of PbS quantum dots for in-vivo high-resolution imaging in the NIR-II window [14]. The doping process can be controlled by modifying the hot injection procedures and adjusting the temperature and mole ratio of PbS [11,15].

Nanostructured materials with unique properties has been produced using ZnS [16]. ZnS nanostructures have one of the richest morphologies among inorganic semiconductors and include nanowires [17], nanorods [18], nanobelts, nanotubes [19], and nanoflowers [20].

Different techniques have been used to produce ZnS thin films and nanostructures. This includes magnetron sputtering [21], ultrasonic spray pyrolysis [22], pulsed laser deposition (PLD) [23], and thermal evaporation. The latter is simple, low-cost and efficient for obtaining nanostructures [24,25].

ZnS nanowires/nanotubes are one-dimensional nanostructures. They have a wide bandgap of 3.6 eV with various applications in photocatalysis [26], sensors [27], and biomedicine [28]. One method for synthesizing ZnS nanowires is the vapor-liquid-solid (VLS) method [29], which uses a metal catalyst (such as Au or Ag) to facilitate the growth of ZnS nanowires from a vapor source. The diameters of ZnS nanowires produced using VLS range from 10 to 200 nm and their lengths can extend up to several micrometers. ZnS

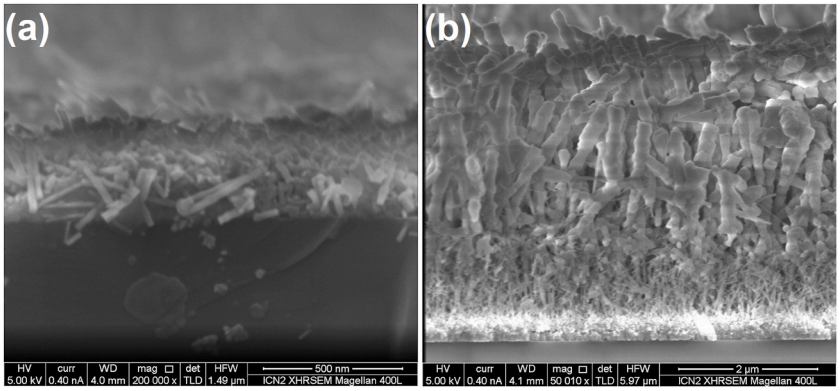

Fig. 2. SEM images representing cross-sectional morphologies for the two samples presented in Fig. 1. (a) sample deposited on Silicon substrate (ZnS/Si) - PbS wt. 12 % (Nanowires); (b) sample deposited on glass substrate (ZnS/glass) - PbS wt. 6 % (Nanorods).

nanotubes are synthesized using a thermochemical process that uses a simple and safe reaction of zinc powder, sulfur powder, and oxygen gas at a high temperature (800 °C) [30]. The thermochemical process can produce ZnS-Zn nanocables, each of which consists of a 20-nm-diameter single-crystal Zn core and an 8-nm-thick polycrystalline ZnS sheath. Evaporation of the Zn core led to the formation of hollow ZnS nanotubes with diameters of 36 nm and lengths of up to several micrometers. Another method for synthesizing ZnS nanotubes is the hydrothermal method [31], which uses an aqueous solution containing a surfactant (such as CTAB) and zinc salt (such as zinc nitrate or zinc acetate) at a low temperature (180 °C) [32]. The hydrothermal method can produce ZnS and/or ZnO nanostructures and nanotubes of various shapes, such as straight, curved, branched, or cross channeled. The diameters and lengths of the ZnS nanotubes depend on the reaction parameters, such as concentration, pH, temperature, and time [33,34].

Light-emitting diodes (LEDs) convert electrical energy into light. ZnS can be used as a shell layer for quantum dots (QDs), which are nanoscale particles that emit light of different colors depending on their size. ZnS can improve the stability and efficiency of QD-LEDs by protecting core QDs from oxidation and quenching [35,36].

In this study, we used a simple thermal-evaporation method to synthesize ZnS nanowires/nanorods using PbS as a dopant. Two samples were prepared using two different concentrations of PbS and two different substrates (glass and Si). The samples were characterized using various techniques including XRD, XPS, SEM, EDX, and HRTEM. The growth mechanism was investigated for optimizing the synthesis parameters.

2. Material and methods

A simple thermal-evaporation technique was used to prepare the samples. 12 wt% (6 %) of PbS powder was added to 88 wt% (94 %) ZnS powder (99.99 % purity) in the crucible as a source material. The distance between the crucible and substrate holder was about 25 cm, the substrate holder was heated before deposition to 200 °C. To investigate the effect of the substrate on the final structures, the samples were deposited on two different substrates: glass and silicon. The deposition process lasted approximately 2.5 h. To ensure the production of high-quality samples, the temperature was gradually increased from room temperature up to 1100 °C during about 30 min. Then the temperature kept constant for 2 h to assure the end of deposition process. The surrounding pressure was 10^{-8} bar.

The crystal structures were determined using XRD. Diffraction patterns were recorded for each sample using a Brucker AXS D8 advanced X-Ray powder diffractometer with a copper target and nickel filter with Cu K_α radiation ($\lambda = 1.540$ Å); measurements were conducted in the range of 20–60° (2θ). Phase identification from the powder diffraction data was performed using the QualX peak identification software [37]. XPS experiments were performed using a SPECS/AES ultrahigh vacuum (UHV) facility. A monochromated Al $_{K\alpha}$ X-ray radiation source (1486.6 eV) operating at 250 W was used. All XPS experiments were performed at room temperature under a base pressure of 10^{-9} bar.

scanning electron microscope (SEM: TSCAN Vega\\XMU model) was used to investigate the morphologies of the obtained structures surface morphology of all samples. For further investigation of the samples, cross-sectional SEM images of the same samples, where the front view of the nanostructure sidewall, were captured and analyzed. The elemental composition of the samples was analyzed using EDX technique.

For HRTEM studies, samples were scratch and immersed in 5 % content of flourhydric acid in water, then were mounted on amorphous carbon grids.

3. Results and discussion

Fig. 1(a–f) shows the SEM images of the surfaces of the prepared samples at different magnifications. Nanostructured materials, covered the surfaces of both samples, as presented in Fig. 1(a–d) (at low magnification). However, at higher magnifications (Fig. 1 (b–e)), different types of nanoclusters were observed in both samples. With a further increase in the magnification power, Fig. 1(c–f), the sample deposited on a silicon substrate (12 wt % PbS) is covered with nanowires, where nanorods cover the other sample deposited

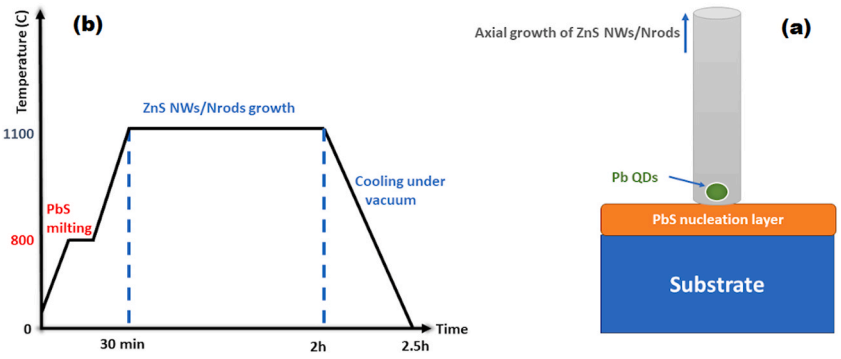

Fig. 3. (a) Proposed schematic diagram of nanowires (NWs)/nanorods (Nrods) growth. (b) The plot of temperature versus deposition time.

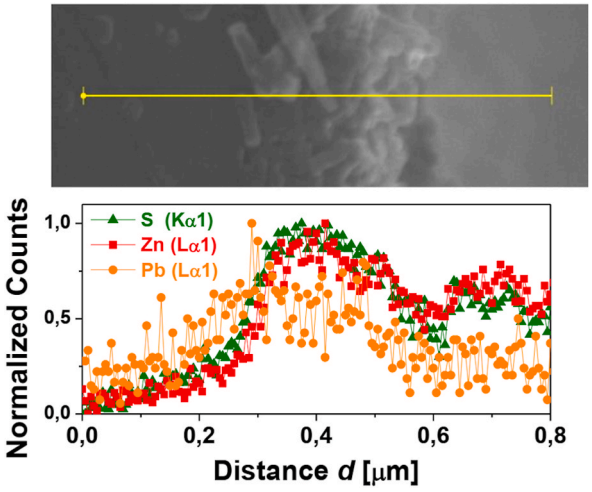

Fig. 4. Cross-sectional elemental profile of deposited ZnS nanowires.

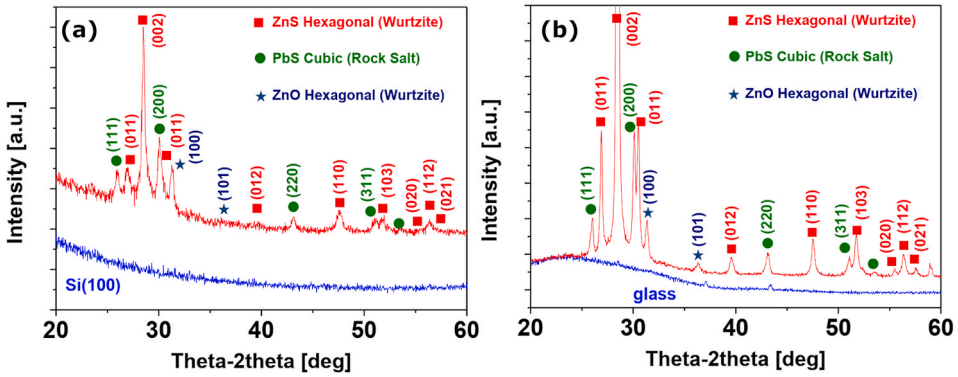

Fig. 5. X-ray diffraction (XRD) patterns of (a) ZnS/Si (12 % wt.% PbS); and (b) ZnS/glass (6 wt% PbS).

on glass substrate (6 wt % PbS). This could be due to the different concentrations of dopant (PbS) in the two samples and substrates, which may lead to different growth mechanisms of the nanoclusters [38].

Fig. 2(a and b) presents the cross-sectional SEM images of the same samples. The morphologies of both samples indicated the formation of cantilever-like nanowires (Fig. 2(a)) or nanorods on top of another thin layer (Fig. 2(b)). During deposition, Pb is expected to form a thin monolayer on top of the substrate, which acts as a nucleation layer for the nanostructures. In our work, we hypothesize that ZnS vapor is swiftly produced at elevated temperatures through the evaporation of ZnS powders. These vapors are then transported and react with the Pb, resulting in the formation of alloy droplets. As the ZnS within the droplets becomes supersaturated, ZnS

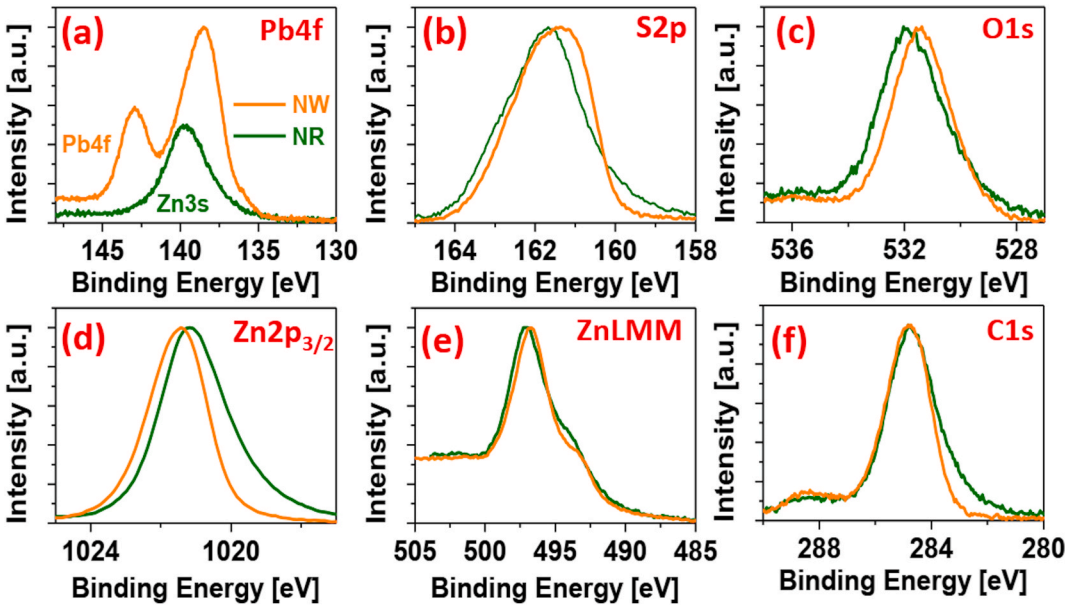

Fig. 6. High-resolution X-ray photoelectron spectroscopy (XPS) spectra in different regions of ZnS composite nanowires (brown)/nanorods (green). (a) Pb 4f, (b) S 2p, (c) O 1s, (d) Zn $2p_{3/2}$, (e) Zn LMM and (f) C 1s peaks.

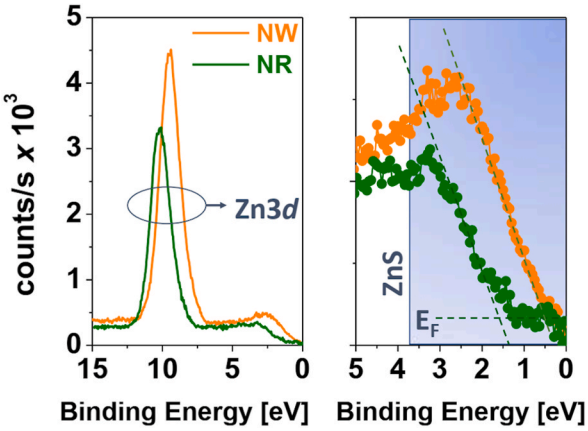

Fig. 7. High-resolution XPS spectra in Zn_{3d} region of ZnS composite nanowires (brown)/nanorods (green).

nanorods or nanowires are generated via a vapor–liquid–solid (VLS) growth mechanism (see Fig. 3(a and b)) [12,13].

It is important to note that in the absence of PbS addition to the ZnS powder during the deposition process, the cross-sectional SEM images of the ZnS thin films reveal a compact structure devoid of nanowires or nanorods as described in Ref. [11].

ZnS nanowires and nanorods have been widely investigated; ZnS nanowires exhibit good field-emission properties, similar to those of conventional field emitters [39]. Li et al. [23] reported an enhancement in the UV near-band-edge (NBE) emission of ZnO by covering the surface of ZnO nanorods with thin ZnS coating.

The Cross-sectional EDX analysis (Fig. 4) revealed that the nanowires/nanorods were composed of zinc and sulfur. The zinc and sulfur contents were almost identical across all the samples, whereas the lead content was much higher at the bottom of the sample than at the top where nanowires/nanotubes were present, indicating that, as expected, lead forms a nucleation layer for the nanowires and nanorods.

The X-ray diffraction (XRD) patterns for the samples synthesized at room temperature are illustrated in Fig. 5(a) for ZnS/Si containing 12 % wt.% PbS, and in Fig. 5(b) for ZnS/glass with 6 wt% PbS. In both samples, the peaks were assigned to three distinct phases. One phase was related to the cubic rock salt structure of PbS, and the other two phases were related to hexagonal (wurtzite) ZnS and ZnO. The nanowires/nanorods preferentially grew along [0 0 2] since the peak intensity corresponding to this orientation was the highest. The intensity and width of the peaks indicate that the sample has a high degree of crystallinity and a small average grain size. The XRD pattern confirmed that the sample was free of impurities and secondary phases. The presence of the ZnO phase was expected,

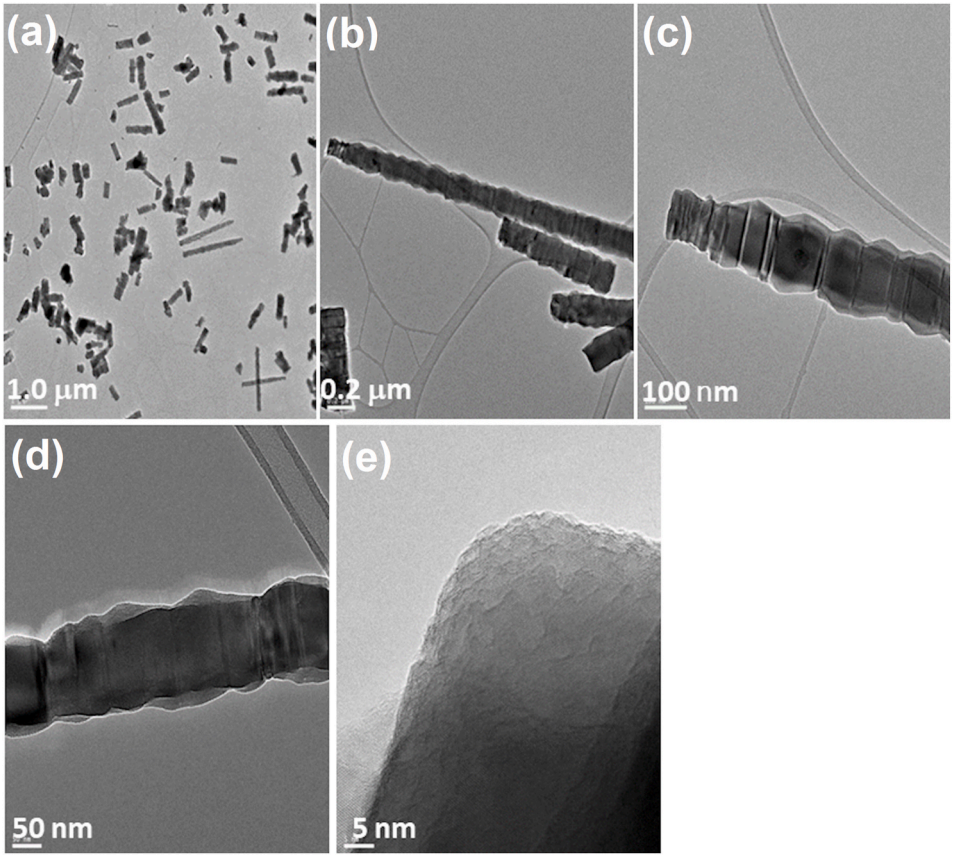

Fig. 8. High resolution transmission electron microscopy (HRTEM) image of ZnS nanorods for different magnifications of the nanoparticles. (a) – 1.0 μm; (b) – 0.2 μm; (c) – 100 nm; (d) – 50 nm; and (e) – 5 nm.

since the vacuum applied was not optimal and a small amount of oxygen may have been present, leading to the formation of the ZnO phase at elevated temperatures. However, the content of this phase was much lower than those of the other phases, as it is clear from the peak intensities in the XRD patterns.

The chemical composition of the surface of the product was investigated using XPS. The XPS results of the ZnS nanostructures yielded information pertaining to the elemental composition, oxidation states, chemical bonding, and surface defects of the nanowires. The XPS profiles were recorded and are presented in Fig. 6(a–f). The spectra show the presence of lead (Fig. 6 (a)), sulfur (Fig. 6(b)), oxygen (Fig. 6(c)), zinc (Fig. 6(e–d)) and carbon (Fig. 6(f)) on the surface of the nanowire sample. In contrast, a signal associated with Pb was detected in the nanorod sample. The Pb_{4f} peaks are located at 143.6 and 139.3 eV and correspond to $Pb_{4f5/2}$ and $Pb_{4f7/2}$ electronic states, respectively. These peaks are associated with the Pb^{+2} oxidation state. The energy difference between the two states was approximately 4.3 eV, which is close to that reported for the $Pb_{4f7/2}$ — $Pb_{4f5/2}$ doublet separation (4.8 eV) in the Pb-doped ZnS NWs system [40]. In the Pb-doped ZnS NWs system, the Pb_{4f} doublet separation indicated the presence and amount of Pb ions in the ZnS nanowires.

Fig. 7 shows the estimated Fermi level (EF) midgap in both ZnS nanowires and nanotubes. Midgap states, the energy levels located within the bandgap of ZnS, can be induced by doping or defects. The presence of midgap states can affect the optical and electrical properties of ZnS. The XPS results indicate that the nanotubes (EF ~1.5 eV) were more insulating than the nanowires (EF ~0.5 eV). This could be due to PbS doping or the formation of Pb QD in the nanowires.

To further examine the nanostructures, HRTEM measurements were carried out over selected regions of both samples. HRTEM is a powerful tool for investigating the morphology, structure, and defects of ZnS nanoparticles and their dopants. The HRTEM images revealed the lattice fringes, interplanar spacings, and crystal phases of ZnS and its dopants. The also revealed the distribution, size, and shape of the nanoparticles, as well as the formation of core-shell structures. These images provide valuable insights into the synthesis, growth mechanism, and property modulation of ZnS nanoparticles via doping. Fig. 8(a–e) shows HRTEM images of the ZnS/glass (PbS 6 wt %) for different magnifications. The images indicate the formation of hexagonal nanorods with lengths of up to a few microns and widths of 100 nm.

Furthermore, EDX Quantification (profile) was conducted to determine the elemental composition of the nanorods along the line of interest, as shown in Fig. 9. EDX Quantification (profile) can provide information about the distribution and concentration of elements in nanoscale structures, such as dopants, interfaces, or alloys. The results showed that the nanorod stoichiometry was almost ideal; a

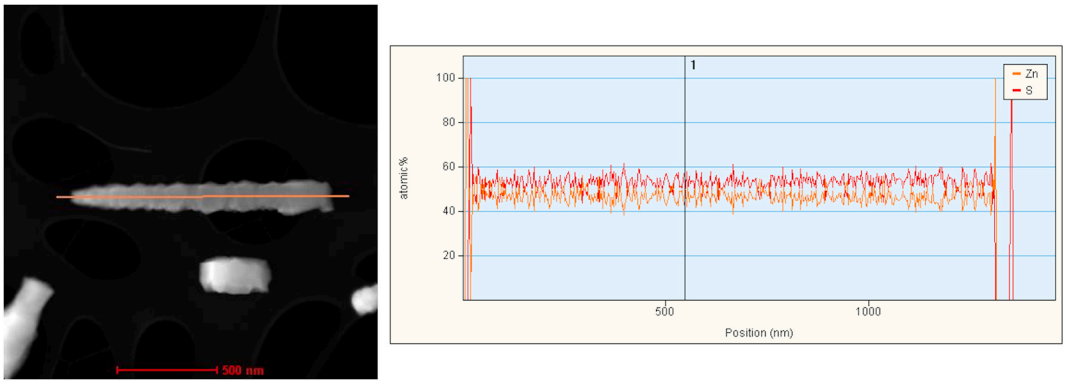

Fig. 9. Energy Dispersive X-ray (EDX) Quantification (profile) of a nanorod along a 1000-nm line.

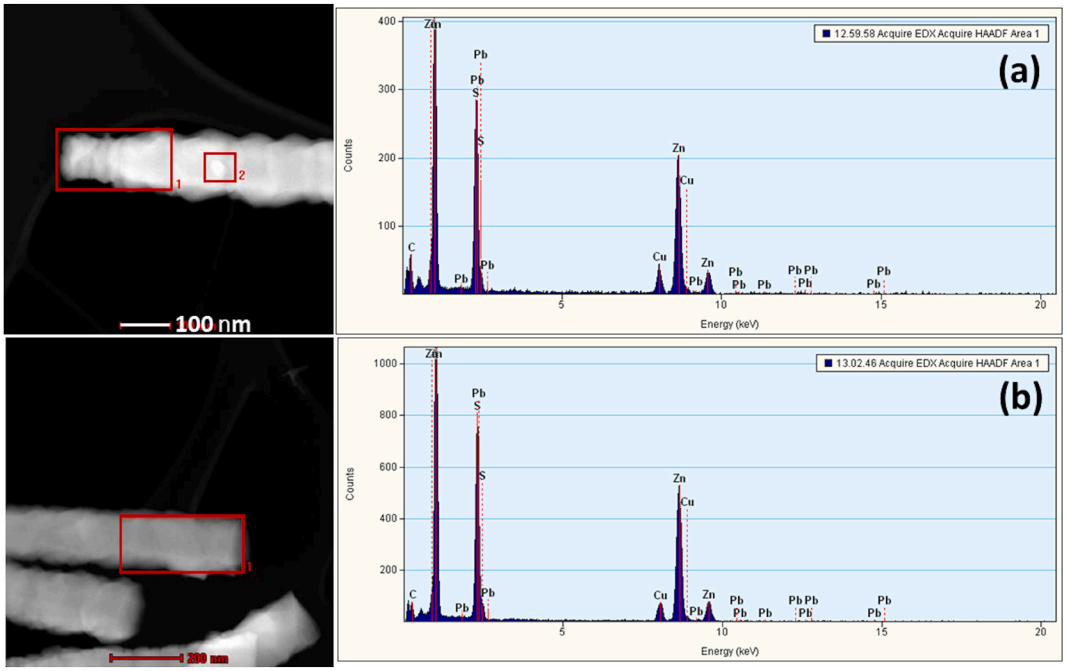

Fig. 10. Energy Dispersive X-ray (EDX) Quantification (area) of (a) the top and (b) the base of the same nanorod as in Fig. 8.

1:1 ratio of zinc to sulfur atoms in the ZnS nanorods did not indicate the presence of other elements (No Pb).

To further investigate the obtained nanorods, EDX quantification (area) measurements were performed on one selected nanorod, and the results are presented in Fig. 10. Two areas were selected on the nanorod: the top (Fig. 10(a)) and the base (Fig. 10(b)). Again, no Pb signal was detected in either region, indicating that the ZnS nanorods were stoichiometric and undoped. These results are consistent with the XPS results, which show no indication of the presence of Pb atoms in the nanorods.

The surface morphology of the ZnS/Si (12 wt % PbS) was examined using HRTEM at different magnifications, as shown in Fig. 11 (a–d). The images show the presence of ZnS nanowires with diameters of approximately 10 nm and lengths of several micrometers. The nanowires had a much smaller diameter than the nanorods in the ZnS/glass sample by a factor of up to ten.

To verify the presence of Pb in the nanowires, EDX Quantification (area) analysis was performed on randomly selected nanowire, as shown in Fig. 12(a–c). Two regions were selected in the nanowire: the top (Fig. 12(a)) and the bottom (Fig. 12(b)). A weak Pb signal was detected in both regions, suggesting that the ZnS nanowires were doped with Pb. This finding is consistent with the XPS results and confirms the successful doping of the nanowires. A spherical structure with a diameter of a few nanometers was at the bottom of the nanowire in the HRTEM image (Fig. 12 (c)). The EDX (area) measurements showed a higher Pb signal in this region than in other regions. This was likely a quantum dot of PbS formed inside the nanowire. PbS quantum dots inside ZnS nanowires are a type of heterostructure that exhibit novel optical and electronic properties. The PbS quantum dots can function as luminescent centers that emit red light under excitation. ZnS nanowires can provide a large surface area and a good carrier transport channel for Pb quantum

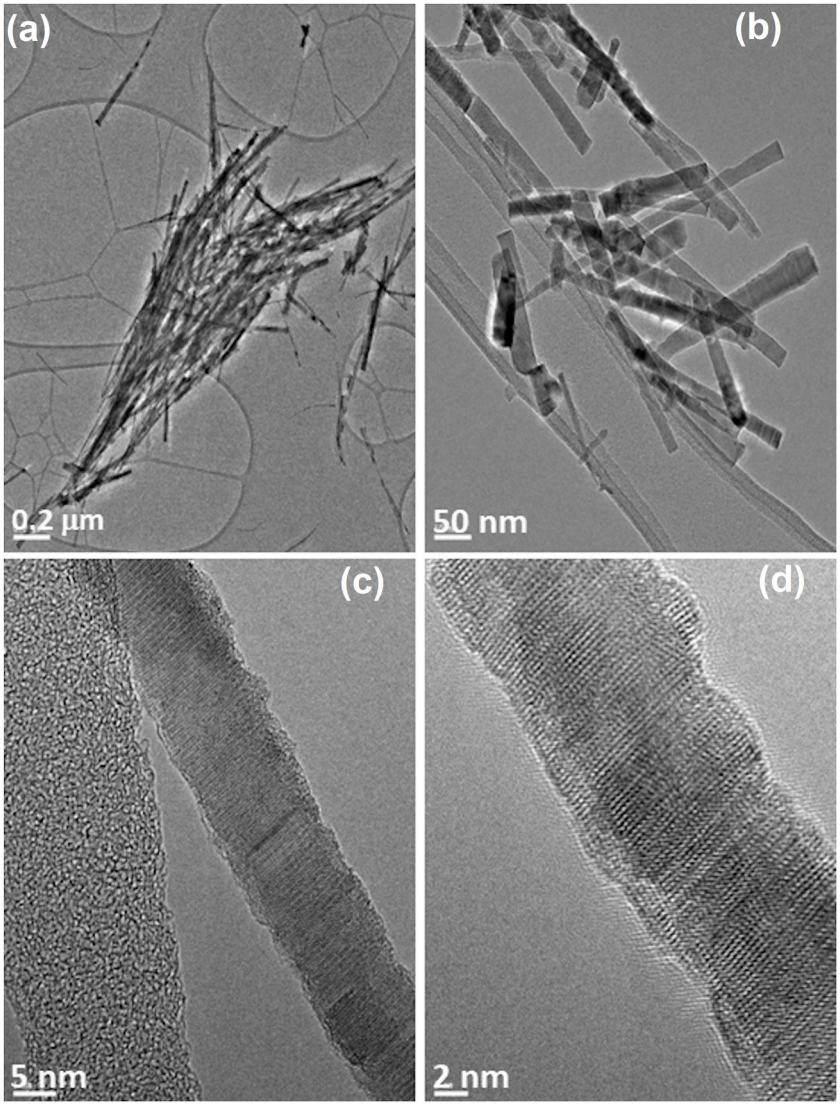

Fig. 11. High resolution transmission electron microscopy (HRTEM) images of ZnS/silicon (12 wt% PbS) for different magnifications. (a) – 0.2 µm; (b) – 50 nm; (c) – 5 nm; and (d) – 2 nm.

dots. The combination of PbS quantum dots and ZnS nanowires can form a direct Z-scheme system that enhances charge separation and transfer efficiency. Moreover, such structures have potential applications in photodetectors, solar cells, and photocatalysts.

4. Conclusions

A simple thermal-evaporation growth method was developed to synthesize ZnS nanowires/nanorods several micrometers in length. Systematic characterization techniques were conducted to determine the structure, morphology, and composition of the obtained nanostructures suing HRTEM and HRSEM. ZnS nanowires/nanorods were grown successfully through thermal evaporation of zinc and sulfur powder at 700 °C using 12 and 6 wt% of PbS as catalyst, respectively. ZnS nanowires/nanorods were grown using a mixture of zinc wurtzite and PbS rock salt. The XPS and EDX mapping spectra showed that nanorods were Pb-free, while nanowires were doped with 5 % Pb. These results indicate the possible formation of PbS Quantum dots within the nanowires, which leads to higher conductivity and n-type character in the nanowires than those in the nanorods. Changing the concentration of the PbS dopant and tuning the parameters that affect the dimensions of the synthesized could improve the properties of the obtained product.

Data and code availability

Not Applicable.

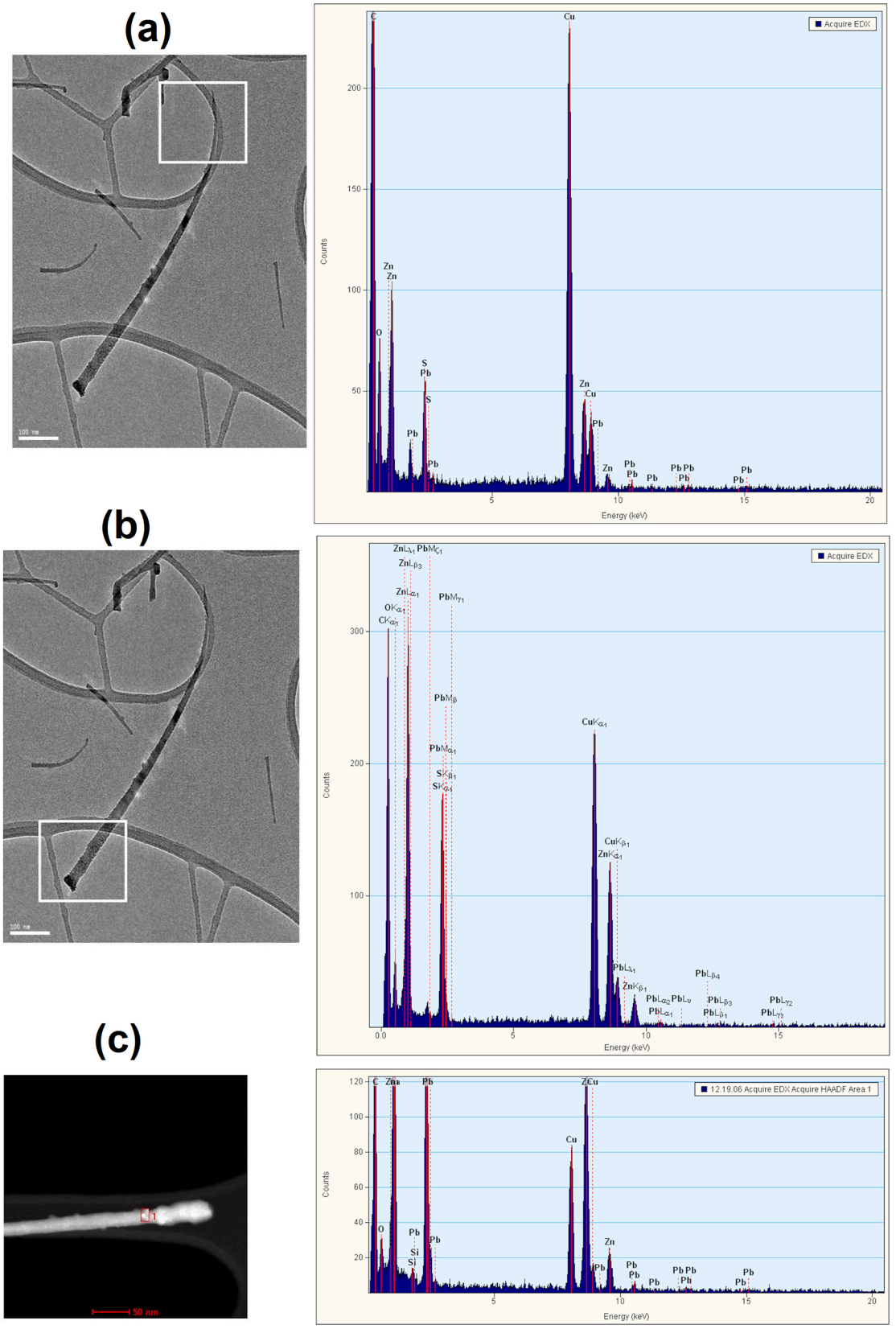

Fig. 12. Energy Dispersive X-ray (EDX) quantification (area) of the (a) top, (b) base the of a nanowire, and (c) QD of PbS inside the nanowire.

Supplementary information

Not Applicable.

Ethical approval

Not Applicable.

Data availability statement

Data included in article/supp. material/referenced in article.

CRediT authorship contribution statement

Bassem Assfour: Writing – original draft, Project administration, Methodology, Conceptualization. **Bassam Abadllah:** Validation, Resources, Data curation. **Nada Daoud:** Software, Formal analysis. **Mahmoud Kakhia:** Visualization, Data curation. **Walaa Zetoun:** Software, Formal analysis.

Declaration of competing interest

The authors declare that they have no known competing financial interests or personal relationships that could have appeared to influence the work reported in this paper.

References

[1] X. Fang, et al., ZnS nanostructures: from synthesis to applications, Prog. Mater. Sci. 56 (2) (2011) 175–287.
[2] S. Tekin, et al., Tuning the linear and nonlinear optical absorption properties of ZnS/hydrochar nanocomposites by concentration of nanoparticles, Opt. Mater. 113 (2021) 110849.
[3] G.-J. Lee, J.J. Wu, Recent developments in ZnS photocatalysts from synthesis to photocatalytic applications—A review, Powder Technol. 318 (2017) 8–22.
[4] J. Rouhi, et al., High-performance dye-sensitized solar cells based on morphology-controllable synthesis of ZnO/ZnS heterostructure nanocone photoanodes, PLoS One 10 (4) (2015) e0123433.
[5] B. Assfour, B. Abdallah, M. Kakhia, Synthesis and characterization of ZnS/PbS quantum dots nanorods array heterostructure, Aerosol Science and Engineering 6 (2022).
[6] H. Krajian, et al., Hydrothermal growth method for the deposition of ZnO films: structural, chemical and optical studies, Microelectron. Reliab. 125 (2021) 114352.
[7] B. Abdallah, et al., Morphological and structural characterization of Pb:ZnS nanostructure films deposited by simple thermal evaporation, Mod. Phys. Lett. B 36 (2021).
[8] V. Ramasamy, K. Praba, G. Murugadoss, Synthesis and study of optical properties of transition metals doped ZnS nanoparticles, Spectrochim. Acta Mol. Biomol. Spectrosc. 96 (2012) 963–971.
[9] L. Chhana, et al., Ab initio investigation of non-metal-doped ZnS monolayer, Appl. Phys. A 127 (9) (2021) 729.
[10] P. Yadav, et al., Metal and non-metal doped metal oxides and sulfides, Green Photocatalysts (2020) 89–132.
[11] B. Muhammad Abdalla, et al., Effect of PbS on ZnS nanostructure deposited using thermal evaporation: growth, morphological and structural study, Iranian Journal of Physics Research 21 (3) (2021) 99–108.
[12] X.-S. Fang, et al., Temperature-controlled catalytic growth of ZnS nanostructures by the evaporation of ZnS nanopowders, Adv. Funct. Mater. 15 (1) (2005) 63–68.
[13] R.S. Wagner, W.C. Ellis, Vapor-liquid-solid mechanism of single crystal growth, Appl. Phys. Lett. 4 (5) (1964) 89–90.
[14] X. Shi, et al., Zn-doping enhances the photoluminescence and stability of PbS quantum dots for in vivo high-resolution imaging in the NIR-II window, Nano Res. 13 (8) (2020) 2239–2245.
[15] B. Assfour, B. Abadllah, M. Kakhia, Synthesis and characterization of ZnS/PbS quantum dots nanorods array heterostructure, Aerosol Science and Engineering 6 (2) (2022) 215–222.
[16] X. Fang, L. Wu, L. Hu, ZnS nanostructure arrays: a developing material star, Adv. Mater. 23 (5) (2011) 585–598.
[17] B. Abdallah, M. Kakhia, W. Zetoune, HRTEM study of ZnS Nanowires films deposited by thermal evaporation, Journal of Nanostructures 10 (4) (2020) 713–722.
[18] M.T. Tran, et al., High-quality optically defect-free 1D ZnS nanostructures by a modified thermal evaporation method, Opt. Mater. 124 (2022) 111963.
[19] M. Bhushan, R. Jha, R. Bhardwaj, Recent strategies and developments of ZnS nanomaterials as photocatalysts and electrocatalysts, in: Advanced Nanomaterials, Springer, 2022, pp. 311–345.
[20] Khan, T.F., et al. Synthesis and Characterization of ZnO-ZnS Nanoflowers for Enhanced Photocatalytic Performance: ZnS Decorated ZnO Nanoflowers. IEEE.
[21] B. Abdallah, M. Kakhia, W. Zetoune, Structural, optical and sensing properties of ZnS thick films deposited by RF magnetron sputtering technique at different powers, World Journal of Engineering 17 (3) (2020) 381–388.
[22] K. Alnama, B. Abdallah, S. Kanaan, Deposition of ZnS Thin Film by Ultrasonic Spray Pyrolysis Effect of Thickness on the Crystallographic and Electrical Properties, 2016.
[23] L. Li, et al., ZnS covering of ZnO nanorods for enhancing UV emission from ZnO, J. Phys. Chem. C 125 (25) (2021) 13732–13740.
[24] P.H. Thach, T.V. Khai, Thermal evaporation synthesis, optical and gas-sensing properties of ZnO nanowires, Crystals 13 (2023), https://doi.org/10.3390/cryst13091380.
[25] N. Hamid, et al., A review on thermal evaporation method to synthesis zinc oxide as photocatalytic material, Nano Hybrids and Composites 31 (2021) 55–63.
[26] G.-J. Lee, J.J. Wu, Recent developments in ZnS photocatalysts from synthesis to photocatalytic applications — a review, Powder Technol. 318 (2017) 8–22.
[27] M. Khawla, et al., ZnS quantum dots as fluorescence sensor for quantitative detection of tetracycline, Opt. Mater. 125 (2022) 112103.
[28] R. Singh, R.R. Singh, Optical Properties of ZnS Quantum Dots: Applications in Solar Cells and Biomedicine, 2022.
[29] Y.-S. Sue, K.-Y. Pan, D.-H. Wei, Optoelectronic and photocatalytic properties of zinc sulfide nanowires synthesized by vapor-liquid-solid process, Appl. Surf. Sci. 471 (2019) 435–444.
[30] M. Guo, et al., Facile and economical synthesis of ZnS nanotubes and their superior adsorption performance for organic dyes, CrystEngComm 19 (17) (2017) 2380–2393.

[31] M. Rauf, et al., Facile hydrothermal synthesis of zinc sulfide nanowires for high-performance asymmetric supercapacitor, J. Saudi Chem. Soc. 26 (4) (2022) 101514.
[32] A. Dumbrava, et al., The influence of Triton X-100 surfactant on the morphology and properties of zinc sulfide nanoparticles for applications in azo dyes degradation, Mater. Chem. Phys. 193 (2017) 316–328.
[33] C.-C. Cheng, et al., Hydrothermal fabrication and characterization of ZnO/ZnS core-shell structures on white reflective films, Results Phys. 10 (2018) 449–457.
[34] S.S. Khudiar, F.A.H. Mutlak, U.M. Nayef, Synthesis of ZnO nanostructures by hydrothermal method deposited on porous silicon for photo-conversion application, Optik 247 (2021) 167903.
[35] R. Li, et al., Facile synthesis of ZnS quantum dots at room temperature for ultra-violet photodetector applications, Chem. Phys. Lett. 742 (2020) 137127.
[36] J. Hao, et al., A facile route to synthesize CdSe/ZnS thick-shell quantum dots with precisely controlled green emission properties: towards QDs based LED applications, Sci. Rep. 9 (1) (2019) 12048.
[37] A. Altomare, et al., QUALX: a computer program for qualitative analysis using powder diffraction data, J. Appl. Crystallogr. 41 (4) (2008) 815–817.
[38] M.-t. Liu, W. Li, Growth and optical property of PbS/ZnS nanocrystals, Superlattice. Microst. 120 (2018) 727–731.
[39] S. Biswas, et al., ZnS nanowire arrays: synthesis, optical and field emission properties, Cryst. Growth Des. 8 (7) (2008) 2171–2176.
[40] A. Osaka, et al., X-ray photoelectron spectroscopy of lead fluorosilicate glasses, J. Mater. Sci. 26 (10) (1991) 2778–2782.